https://doi.org/10.1007/s00348-018-2491-6

Phosphor thermometry on a rotating flame holder for combustion applications

Pradip Xavier[1,2] · Laurent Selle[1] · Gorkem Oztarlik[1] · Thierry Poinsot[1]

Abstract

This study presents a method to measure wall temperatures of a rotating flame holder, which could be used as a combustion control device. Laser-induced phosphorescence is found to be a reliable technique to gather such experimental data. The paper first investigates how the coating (thickness, emissivity and lifetime) influence the flame stabilization. While the low thermal conductivity of the coating is estimated to induce a temperature difference of only 0.08–0.4 K, the emissivity increases by 40%. Nevertheless, the transient and steady-state flame locations are not affected. Second, because temperature measurements on the rotating cylinder are likely to fail due the long phosphor lifetimes, we modify the classical point-wise arrangement. We propose to illuminate a larger area, and to correct the signal with a distortion function that accounts for the displacement of the target. An analytical distortion function is derived and compared to measured ones. It shows that the range of measurements is limited by the signal extinction and the rapid distortion function decay. A diagram summarizes the range of operating conditions where measurements are valid. Finally, these experimental data are used to validate direct numerical simulations. Cylinder temperature variations within the precision of these measurements are shown not to influence the flame location, but larger deviations highlight different trends for the two asymmetric flame branches.

1 Introduction

Performances and durability of combustion systems have been tremendously improved since Whittle's first turbojet, and regulations for pollutant emissions, noise and fuel consumption are driving future optimization and technological developments (Wulff and Hourmouziadis 1997; Lawrence 2009). Thermal efficiency improvement is crucial but limited by the thermal resilience of nozzle guide vanes used in gas turbines (Lefebvre 1999; Facchini et al. 2004; Duchaine et al. 2009; Berger et al. 2016). Moreover, the compactness of future systems is likely to enhance material stresses (Dreizler and Bohm 2015). The development of new materials that can withstand higher temperatures, raises the need to better understand their behavior in a combustion environment (Padture et al. 2002; Hooker and Doorbar 2000). Among others, flame–wall interactions and subsequent heat transfer in a combustor need to be carefully addressed as they can influence pollutant formation (Popp and Baum 1997; Mann et al. 2014; Jainski et al. 2017), flammability limits (Lakshmisha et al. 1991; Lamouroux et al. 2014; Xavier et al. 2017), flame stability (Guiberti et al. 2015; Mercier et al. 2016; Berger et al. 2016) or combustion instabilities (Tay-Wo-Chong 2013; Mejia et al. 2015; Kraus et al. 2017).

Wall temperature measurements in combustion systems are therefore mandatory but remain challenging due to the high-temperature and corrosive environment (Dreizler and Bohm 2015). Classical thermometry techniques suffer from several drawbacks. Thermocouples are intrusive and have their own thermal inertia, infrared thermometry (IR) relies on the knowledge of the material emissivity and the signal suffers from interferences with light emission from the flame (chemiluminescence). Thermal paints only provide

✉ Pradip Xavier
pradip.xavier@imft.fr; pradip.xavier@coria.fr

Laurent Selle
laurent.selle@imft.fr

Gorkem Oztarlik
gorkem.oztarlik@imft.fr

Thierry Poinsot
thierry.poinsot@imft.fr

[1] Institut de Mécanique des Fluides de Toulouse (IMFT), Université de Toulouse, CNRS, Toulouse, France

[2] Present Address: CORIA-UMR 6614, Normandie Université, CNRS, INSA et Université de Rouen, Campus Universitaire du Madrillet, 76800 Saint-Etienne du Rouvray, France

mean or peak information (Lempereur et al. 2008). Phosphor thermometry has appeared to be an interesting trade-off for these applications. Being semi-invasive as it requires to add a thin coating of phosphor particles, this technique—often named laser-induced phosphorescence (LIP)—uses rare-earth-doped ceramic phosphors whose spectroscopic properties are highly sensitive to temperature (Allison and Gillies 1997; Khalid and Kontis 2008; Chambers and Clarke 2009). In practice, this technique can be either implemented in the temporal domain, by measuring the phosphorescence glowing after excitation (Knappe et al. 2012), or in the spectral domain, by estimating a ratio of intensities (Feist et al. 2002). Fuhrmann et al. (2013) performed a systematic study of these two approaches and showed the advantages of the lifetime method, which is used in this study.

Despite the numerous applications of this technique to combustion (Kashdan and Bruneaux 2011; Alden et al. 2011; Brubach et al. 2013), some authors have studied how the surrounding environment can alter the spectroscopic properties of these particles. As an example, Brubach et al. (2013) investigated the influence of the dopant concentrations, laser energy, surrounding gas composition and pressure rise on a thermographic phosphor. However, to the authors' knowledge, the influence of this coating on flame stabilization has received little attention. For example, the coating is likely to change the material emissivity, the radiative heat transfer, the flame stabilization, and could even alter its stability (Miguel-Brebion et al. 2016; Kraus et al. 2017). This aspect will be treated in the first part of this paper.

Recently, Mejia et al. (2017) highlighted the possibility to perform active control of thermoacoustic instabilities of a flame stabilized on a rotating cylindrical flame holder. Xavier et al. (2017) numerically showed that the corresponding heat fluxes were more than three times larger, in comparison to classical flame–wall interaction cases (Poinsot and Veynante 2011; Ezekoye et al. 1992; Lu et al. 1990). The lack of detailed measurements in Mejia's experiment was the motivation for the implementation of LIP on this configuration. However, the rotating flame holder raises some questions on the data analysis: the classical point-wise laser excitation is likely to fail if the displacement of the moving target during the phosphorescence decay is larger than the typical size of the illuminated area. Several studies on moving surfaces have been reported, and the classical strategy consists in using phosphors with fast decay lifetimes (Mannick et al. 1987; Allison et al. 1988; Tobin et al. 1990; Alden et al. 2011). Thus, the object can be considered as a quasi-static object during the collection process. However, because this solution requires specific phosphors with adequate hardware, the authors want to evaluate the capabilities of a phosphor with longer decay lifetimes, by slightly modifying the point-wise static arrangement (second part of the paper).

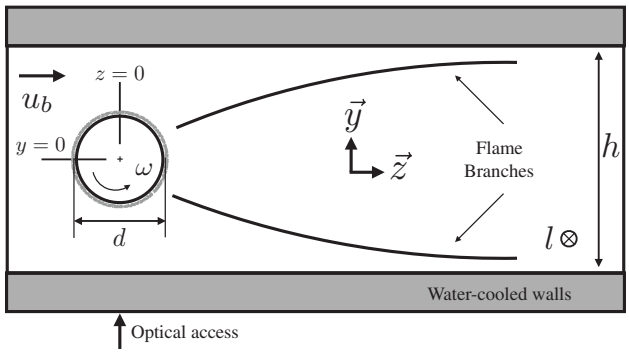

Fig. 1 Longitudinal cut through the combustion chamber (front view) and definition of the control parameters

The aim of this study is twofold: (1) evaluate the influence of the coating on the flame stabilization, and (2) provide a simple methodology for measuring temperatures on fast rotating parts with a phosphor having long decay lifetimes. Derived from the classical point-wise LIP arrangement, the methodology is implemented on the canonical case of a flame stabilized on a rotating cylindrical flame holder (Mejia et al. 2017).

The paper is organized as follows: the combustion test bench is briefly introduced in Sect. 2 while LIP implementation and validation are discussed in Sect. 3. Finally, the methodology for measuring temperatures on the rotating flame holder is described and validated in Sect. 4.

2 Setup and diagnostics

2.1 Combustion chamber

This study is performed on a confined laminar premixed methane/air flame, stabilized in the wake of a cylindrical flame holder. The setup, which is the same as that of Xavier et al. (2017), consists of a constant-section channel with a rectangular cross section: height, $h = 37$ mm and depth, $l = 94$ mm (cf. Fig. 1). The flame holder is a stainless-steel cylinder of diameter, $d = 8$ mm, which can be rotated at a constant angular velocity, ω, by a brushless electric engine (Faulhaber 2232S024BX4).The front side of the burner is equipped with a quartz window to allow direct flame visualization and the lateral walls are fitted with two optical slits for the passage of a laser sheet (not shown). The lateral walls are also water-cooled, which helps reducing the thermal inertia of the setup and allows a precise specification of boundary conditions for numerical simulations.

The bulk velocity and the equivalence ratio of the mixture are $u_b = 1.07$ m/s and $\phi = 0.7$, respectively. The Reynolds number, based on the cylinder diameter and the bulk velocity is $Re = 580$. In this regime, the reacting flow is steady.

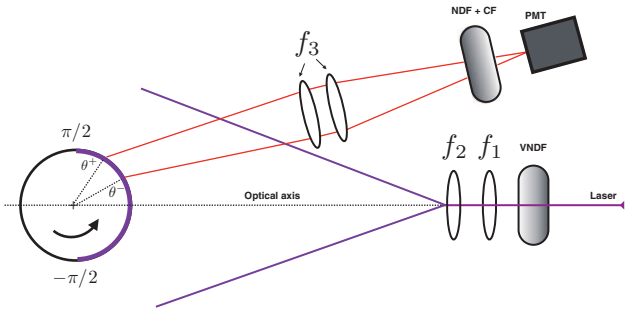

Fig. 2 Optical arrangement of the rotating laser-induced phosphorescence in the case of rotating cylinder. *VNDF* variable neutral density filter; *NDF* neutral density filter; *CF* colored filter; *PMT* photomultiplier; f_1 spherical lens (1000 mm); f_2 cylindrical lens (−22 mm); f_3 spherical lens (500 mm)

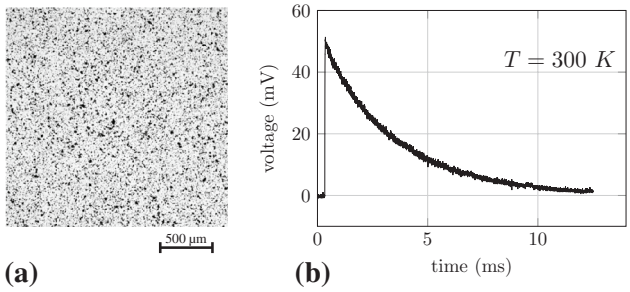

Fig. 3 **a** Microscopic image of the coating (binder+phosphor particles). **b** Typical phosphorescence decay curve obtained at room temperature $T = 300$ K

The control parameter of this experiment is the normalized rotation rate, α, defined as

$$\alpha = \omega d/2u_b. \tag{1}$$

The cylinder rotation speed ranges from 380 to 7600 rpm (rotation per minutes), corresponding to values of α between 0.15 and 3.

2.2 Laser-induced phosphorescence (LIP)

One objective of this study is to measure the temperature of the flame holder when it is rotating, via laser-induced phosphorescence. One issue with the classical point-wise laser excitation is that it is likely to fail if the phosphorescence decay time is much larger than the time the sensor views the illuminated spot. For instance, a rotating cylinder with $\alpha = 2$ (i.e., 5100 rpm) at room temperature has a displacement of ≈ 7 mm while the phosphor decays. This is definitely larger than the sensor field of view, which will experience a rapid signal extinction. Instead of using fast decay lifetimes' phosphor, the present setup produces a laser sheet rather than a point-wise excitation. Besides the increased collected signal, this solution also extends the phosphorescence collection time. Figure 2 presents the optical bench that can be applied to both steady and rotating cylinders. The laser beam first goes through a convergent lens ($f_1 = 1000$ mm) and is expanded through an additional cylindrical diverging lens ($f_2 = -22$ mm). Its optical axis is normal to the flame holder's rotation axis, so that the plane illuminates half of the cylinder's perimeter. The phosphorescence signal is collected on a set of two spherical lenses (diameter 50 mm, $f_3 = 500$ mm) and which increases the collected light on a photomultiplier (PM) tube (Hamamatsu H7422-50). The backward collection configuration is slightly tilted from the optical axis (Fig. 2). Because the cylinder is in the object plane of the first spherical lens, the PM sees a part of the cylinder. The viewing area is determined experimentally by replacing the pulsed laser source by a continuous diode source. The reflected light is collected on the PM and a mask is displaced in the streamwise direction until signal extinction occurs. The maximum amplitude of displacement is therefore converted to two angles, θ^- and θ^+. In this study, $\theta^- = 0.5$ rad and $\theta^+ = \pi/2$ rad, meaning that the PM sees the upper part of the cylinder.

Preliminary measurements using infrared thermography and thermocouples have shown that the temperature range for the steady flame holder lies between $T = 500$ K and $T = 800$ K for typical operating conditions. Therefore, we chose the commercial powder $Mg_4\,FGeO_{5,6}:Mn$ (Osram SV067), which has an operating range from 300 to more than 900 K, corresponding to phosphor lifetimes from 3.3 ms to 5 µs (Brubach et al. 2008). The median diameter of the particles lies between 5.8 and 10.5 µm. The phosphor particles are mixed with a liquid ceramic binder (Zyp Coatings, Inc., HPC). The phosphor mass concentration is set to 5 % in this study, providing signal-to-noise ratios larger than 30 between 300 and 850 K (based on the maximum signal intensity and the mean background noise, see Fig. 3b). The resulting mixture is sprayed on the cylinder with an airbrush (Sotar Super Micron).

This coating is excited with the third harmonic (355 nm) of a Nd:YAG pulsed laser (at 10 Hz). The laser pulse energy is adjusted to 30 µJ per shot with a variable neutral density filter (Thorlabs NDC-50C-4-A). This level is in the linear range for the response of the coating and is low enough to prevent thermal damage (Atakan and Roskosch 2013; Linden et al. 2009). The PM is equipped with neutral density filters to prevent photocathode saturation (Brubach et al. 2008), and a set of colored optical filters: residuals from the laser excitation are removed with a high-pass filter (CVI LPF-550). The phosphorescence signal is transmitted by means of a narrow band-pass filter (CVI F10-660) at 660 ± 10 nm. The current output from the PM goes through an in-house current-to-voltage converter (load resistance of 10 kΩ) and is recorded by a 1 MHz acquisition card.

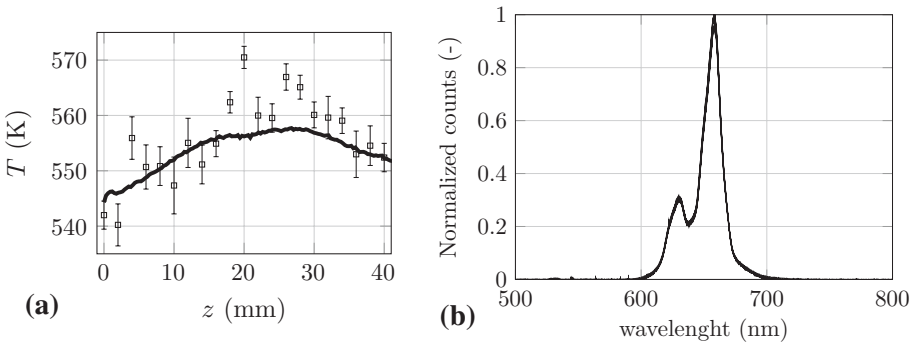

Fig. 4 **a** Comparison of the transverse temperature across the heated sample, between LIP data (square) and infrared thermography (solid line). **b** Series of ten emission spectra taken at room temperature (300 K) and spaced by a heating period of 10 min at 900 K between each measurement

3 Signal processing and validation

Measurements are performed in the temporal domain, by recording the phosphorescence decay after the coating has been excited by the laser. The collected signal is normalized by its maximum and a portion of the curve (between 10 and 90 % of the maximum) is extracted to get rid of fast fluorescence processes after the laser excitation and background noise when the signal has sufficiently decayed. Thus, the extracted data are fitted with an exponential function:

$$I(t) = \mathrm{e}^{-t/\tau}. \tag{2}$$

The principle of LIP is that the decay time τ depends on the temperature, T, of the material. A calibration procedure is required to establish the relation, $T(\tau)$, between the temperature and the decay time. For this calibration, we use a stainless steel heated sample by means of two heating cartridges, and whose temperature is controlled by a type K thermocouple. The sample temperature ranges from 300 to 850 K. For each temperature, 100 laser shots are recorded and the mean curve is fitted to estimate τ. The number of required data is determined by a sensitivity analysis to statistically converge the 1st and 2nd moments of τ. Prior to each measurement campaign, a calibration is performed on a newly coated sample.

The precision of the data is evaluated during the calibration procedure. For each temperature, the standard deviation due to shot-to-shot variations is converted to a temperature shift. This procedure is repeated over the entire range of temperature, which results in a precision of ± 7 K. The accuracy is determined by a comparison with infrared thermography. Figure 4a shows the transverse temperature profile across the sample with the two measurement methods. The infrared thermography measurements have an averaged standard deviation of 0.1% (not depicted in Fig. 4a), so that the mean IR temperature is used as the baseline for estimating the LIP accuracy. The averaged discrepancy (i.e., the average error) of the LIP to IR measurements is $\sim 1\%$.

The application of the coating is delicate and it is anticipated that it could be be user-dependent. Therefore, a series of tests is conducted to validate the coating technique. These tests are conducted on a coated piece of glass so that the distribution of phosphor particles can be visualized. The piece of glass is coated with the same procedure as the sample and the quality of the deposit procedure is checked with an upright transmission microscope (Zeiss A1 coupled with a $2000 \times 2000\,\mathrm{pix}^2$ Basler ace camera). A raw visualization of 2 by 2 mm^2 (Fig. 3a) shows that the airbrush technique produces a rather homogeneous coating. An example of a phosphorescence decay curve in Fig. 3b confirms the excellent signal-to-noise ratio with the settings described in Sect. 2.2. Without any specific procedure during the application, the airbrush technique produces a homogeneous coating while being inexpensive compared to more elaborated techniques (Brubach et al. 2013). The coating thickness is evaluated with a contact measurement gauge λ-Logitech (precision of ± 0.1 µm). 40 point-wise measurements distributed over the sample gives an averaged thickness of 10 µm with a standard deviation 1 µm. The linear trend observed when applying several layers (i.e., a slope of 10 µm per layer) proves the good repeatability of the technique. The cylinder is coated while it is rotating at low speed, to ensure a good uniformity.

We anticipate that the coating may be altered or damaged by the harsh conditions of the reacting flow. to reproduce typical experimental conditions, several cycles of heating load are conducted: the sample is heated to 900 K during 10 min, and this procedure is repeated ten times. Between each heating load, an emission spectrum is recorded on a spectrometer (Ocean Optics USB 2000+, wavelength range from 330 to 1100 nm, optical resolution of 0.3 nm). Figure 4b presents ten successive spectra which have been normalized by the maximum of the first one. Both shape and amplitude of the spectra do not change with time so that neither spectroscopic nor signal-to-noise ratio are affected. An additional visual inspection confirms the excellent thermomechanical resistance to heat loads. It is therefore concluded that this coating is adequate for repeated use under reacting conditions, without measurable alteration of its performance.

The stabilization of the flame is known to depend on the material temperature, which is driven by the conductive and radiative properties of the flame holder. Knowing that the low thermal conductivity of the coating ($\lambda \approx$

Table 1 Emissivity of a polished stainless steel ϵ_p and a phosphor coating ϵ_c when varying temperature

T (K)	ϵ_p	ϵ_c
473	0.27	0.38
523	0.26	0.38
573	0.25	0.39

1–5 W/m K) can produce a temperature difference between the cylinder temperature, T_c, and the measurement, T_{LIP}, we use a simple resistance model to evaluate this shift, $\Delta T = \Phi R$ (the heat flux Φ is obtained from numerical simulations (Xavier et al. 2017), and R is the thermal resistance). The estimated temperature difference of 0.08–0.4 K is much lower than the precision of the technique and is not expected to play a major role in the flame stabilization process (Sect. 4.2). We also investigate the modification of the emissivity by the coating. Even if the coated surface is usually small, it might affect heat transfer and the flame location (Miguel-Brebion et al. 2016). The emissivity of the calibration sample's raw surface is compared to a coated one. The emissivity at a given temperature is,

$$\epsilon(T) = \frac{L(T) - L_e(T_e)}{L_0(T) - L_e(T_e)}, \tag{3}$$

where L is the luminescence of the surface (either raw or coated), L_0 is the luminescence of a black body (DCN 1000 N4, NHG), and L_e is the luminescence reflected from the environment at room temperature T_e. The transmission of air between the camera and the object is neglected as measurements are performed with a 14-bit infrared camera (Jade MWIR, CEDIP) operating with a spectral range of 3.6–5.2 µm, which corresponds to a high air transmittance window. The integration time is set to 20 µs to prevent sensor saturation at high temperatures.

Results are given in Table 1, where ϵ_p and ϵ_c are the emissivities of the raw and coated surface, respectively. The coated surface has an emissivity ~ 40% larger than the raw one: the coating application increases the wall roughness, which could be the main reason for the increased emissivity (not discussed here).

Because of the significant increase in ϵ, an a posteriori study is conducted: the influence of the coating on the flame anchoring location is conducted by temporally tracking the flame root location (FRL) of both branches. First, an uncoated cylinder is used as the reference for the FRL. Then, the cylinder is fully coated with the phosphor thereby varying the number of coating layers (from one to four layers). The flame is imaged on a Image Intense camera (LaVision), equipped with a $f/16$ 182 mm telecentric lens (TC4M64, Opto-engineering) to better resolve the vicinity of the cylinder. A colored optical filter, centered at 430 ± 10 nm, is placed in front of the sensor to collect the spontaneous CH* emission. Figure 5 presents the FRL (average of the two branches) during the transient heating. CH* chemiluminescence images are collected and the exact FRL is detected with a crest detector. After 400 s, the FRL has reached a steady state position. A slight difference is observed between the uncoated and the coated cylinder. The FRL of the coated cylinder is shifted downstream by approximately $0.35\delta_L^0$ (δ_L^0 is the planar unstretched adiabatic flame thickness), in comparison to the uncoated one. Modifications of the aerodynamics around the cylinder induced by the roughness of the coating and alteration of radiative properties would play a combined role to displace the steady-state flame stabilization. Moreover, increasing the number of layers does not change the FRL obtained for one layer. We therefore conclude the coating used in this study—especially the emissivity modification—is not significantly affecting the transient and steady flame stabilizations.

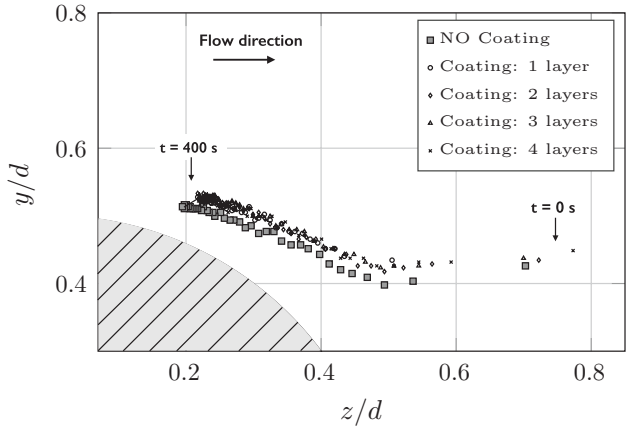

Fig. 5 Evolution of the flame root with time without rotation, for an uncoated cylinder (gray rectangles) and a coated cylinder (several layers)

4 Results

In Sect. 3, the LIP technique was calibrated on a non-rotating cylinder and it was checked that the coating did not affect the flame. In this section, the methodology for LIP measurement on the rotating cylinder is presented. As explained in Sect. 2.2, half of the perimeter is illuminated by the laser sheet and phosphorescence viewed by the photomultiplier is collected. Consequently, this setup measures the average temperature on the cylinder's surface. However, as the Biot number is 0.01, no temperature gradients are expected in the cylinder. Moreover, when the cylinder is rotating with $\alpha > 0.2$, the thermal time scale $\tau_s = d^2/D$ (D is the thermal diffusivity) is 6 s, which is 50 times larger than the rotation time scale $\tau_r = \pi d/\alpha u_b$

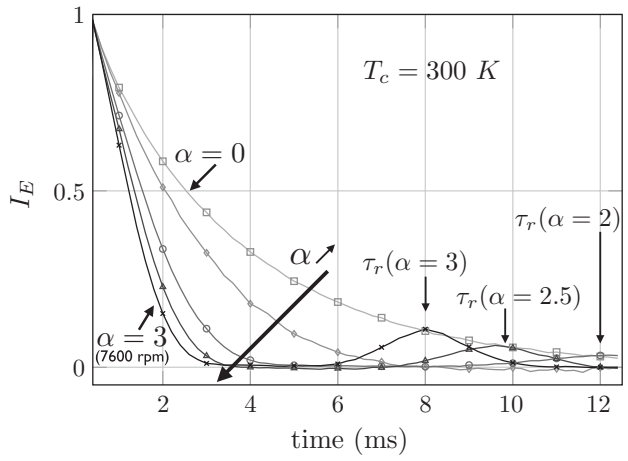

Fig. 6 Evolution of phosphorescence raw signals for different rotation rates α, without combustion, i.e., at room temperature $T_c = 300\,\mathrm{K}$. The secondary peak in the signal corresponds to the time τ_r for a full revolution of the cylinder

(one cylinder revolution). Thus, the temperature uniformity is enhanced by rotation.

4.1 Distortion function determination

Figure 6 shows typical phosphorescence signals recorded at ambient temperature (i.e., without flame) and for different rotation rates, α. For $\alpha = 0$, the signal exhibits an exponential decay. However, when α increases, the decay rate is smaller than without rotation because a portion of the illuminated area moves out of the PM field of view (i.e., signal extinction). This leads to a systematic error in the evaluation of the temperature because the LIP relies on the knowledge of a calibration curve $T(\tau)$ obtained without rotation. At high rotation rates ($\alpha > 2$), the cylinder performs a full revolution during the phosphorescence decay so that the PM signal goes to zero (when the cylinder has performed half of a revolution) and presents a secondary peak when the illuminated area has done a full revolution. It is therefore obvious that when LIP is performed on the rotating cylinder, a correction factor must be applied to the PM signal. We now propose an analytical evaluation of the distortion function, $\gamma(t, \alpha)$, that relates the phosphorescence signal when the cylinder is moving, $I(t, \alpha)$, to the one without rotation, $I(t, \alpha = 0) = I_0(t)$.

Figure 7a represents the portion of the cylinder that is illuminated by the laser sheet. As the diverging lens is 2 m away from the cylinder, the laser fluence I_L, received on the cylinder surface is assumed to be uniform between $-\pi/2$ and $\pi/2$.Consider a portion dl of the cylinder's surface, at an angle θ from the direction of the laser axis. The intensity received from the laser $\mathrm{d}I_\mathrm{R}$ is

$$\mathrm{d}I_\mathrm{R} = I_\mathrm{L}\cos(\theta)\mathrm{d}l. \tag{4}$$

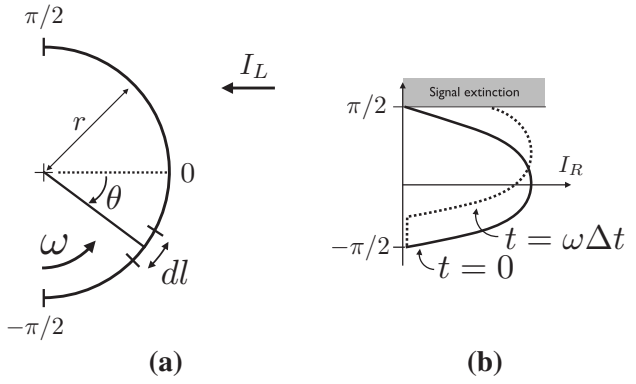

Fig. 7 Schematic representation of the modified LIP setup. **a** Definition of the different parameters. **b** Advection of the azimuthal intensity I_R received from the laser

Because the LIP is operated in the linear regime, the phosphorescence emission $\mathrm{d}I_\mathrm{E}$ is proportional to the intensity received

$$\mathrm{d}I_\mathrm{E} = \beta I_\mathrm{L}\cos(\theta)\mathrm{e}^{-t/\tau}\mathrm{d}l, \tag{5}$$

where β accounts for linearity between $\mathrm{d}I_\mathrm{R}$ and $\mathrm{d}I_\mathrm{E}$. Because the PM is almost aligned with the optical axis of the laser, it collects the phosphorescence with an angle $\theta - \omega t$ (Fig. 7b). The term ωt accounts for the cylinder rotation. A Lambertian pattern (i.e., the off-normal emitted radiance follows a cosine law) is considered for the phosphorescence scattering, based on Allison and Gillies (1997) and Lee et al. (2007). Combining Eqs. (4) and (5) gives

$$\mathrm{d}I_\mathrm{E} = \beta I_\mathrm{L}\cos(\theta - \omega t)\cos(\theta)\mathrm{e}^{-t/\tau}\mathrm{d}l. \tag{6}$$

Since $\mathrm{d}I_\mathrm{E}$ is an amount of light, negative values must be discarded. This is performed with a sliding Heaviside step function $H(\theta)$,

$$\mathrm{d}I_\mathrm{E} = \beta I_\mathrm{L}\mathrm{e}^{-t/\tau}\cos(\theta - \omega t)\cos(\theta)H(\theta + \pi/2 - \omega t)\mathrm{d}l. \tag{7}$$

The signal collected on the PM is the integral of $\mathrm{d}I_\mathrm{E}$ over the field of view of the sensor (cf. Fig. 2):

$$I(t, \alpha) = \int_{\theta^-}^{\theta^+} \mathrm{d}I_\mathrm{E}, \tag{8}$$

where θ^+ and θ^- represent the maximum angles of the PM's field of view. Using the cylindrical coordinates (i.e., $dl = rd\theta$) yields,

$$I(t, \alpha) = r\beta I_\mathrm{L}\mathrm{e}^{-t/\tau}\int_{\theta^-}^{\theta^+}\cos(\theta - \omega t)\cos(\theta)H(\theta + \pi/2 - \omega t)\mathrm{d}\theta. \tag{9}$$

Using Eq. (9), it is possible to define the distortion function $\gamma(t, \alpha)$, which is the ratio of the signal with rotation, $I(t, \alpha)$, and the one without rotation $I(t, \alpha = 0) = I_0(t)$,

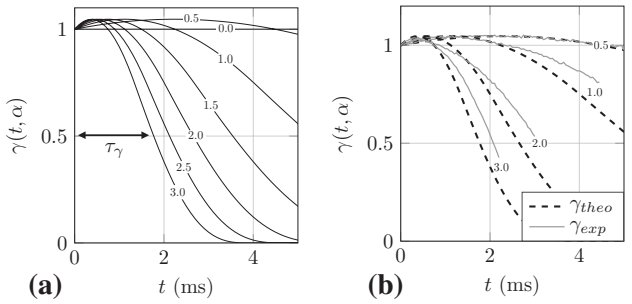

Fig. 8 **a** Theoretical efficiency function $\gamma(t,\alpha)$ from Eq. (10) for different α. **b** Evaluation of efficiency functions γ from theory (Eq. (10)) and experiments ($I(t,\alpha)/I(t,\alpha=0)$), taken for several rotation rates α

$$\gamma(t,\alpha) = \frac{I(t,\alpha)}{I_0(t)} = \frac{\int_{\theta^-}^{\theta^+} \cos(\theta-\omega t)\cos(\theta)H(\theta+\pi/2-\omega t)\mathrm{d}\theta}{\int_{\theta^-}^{\theta^+} \cos^2(\theta)d\theta}. \tag{10}$$

Equation (10) shows that the distortion function, $\gamma(t,\alpha)$, only depends on the PM's field of view and the cylinder's rotation rate.[1] Equation (10) can be numerically integrated so that a phosphorescence signal recorded on the rotating cylinder can be corrected for the rotation via the distortion function. Figure 8a shows the theoretical distortion functions for different rotation rates α. Obviously, the non-rotating case leads to a unit distortion function. When rotation is imposed, a slight overshoot above unity occurs before the function drops to zero: because the PM sees the upper part of the cylinder (positive θ), it records, with a delay, the maximum phosphorescence emitted at $\theta = 0$. As the rotation rate increases, $\gamma(t,\alpha)$ drops more rapidly, confirming the signal extinction due to the rotation. The theoretical distortion function that is determined in the previous section can be validated by directly measuring the ratio of phosphorescence signals $I(t,\alpha)/I_0(t)$. However, this test needs to be done at the same temperature. In our experiment, the ambient condition at $T_c = 300\,\mathrm{K}$ is the only one that ensures a constant cylinder temperature. Indeed, as shown by Xavier et al. (2017), the steady-state temperature of the cylinder under reacting conditions depends on the rotation rate. The comparison between theory and experiments in Fig. 8b shows an excellent agreement for $\alpha = 0.5$. However, discrepancies occur for larger rotation rates, which are not fully understood.

As the rotation increases, the time the PM sees the illuminated area $\tau_c = (\pi/2+\theta^+)r/\alpha u_b$ is shortened. If the phosphorescence decay is longer than the PM collection time (i.e., rotation timescale τ_c), it will clearly induce a bias, by reducing the fitting window (Tobin et al. 1990). Thus, one must ensure that the phosphorescence decay time $\tau_P = \ln(10)\tau$ (τ being the phosphorescence lifetime) is much smaller than the rotation timescale τ_c to prevent any information losses. Similarly, the correction we propose induces a post-processing bias as the recorded signal $I(t,\alpha)$ is divided by the efficiency function γ which tends to zero. With the intent to define the validity range of the correction procedure, we arbitrarily define τ_γ as the time at which the distortion function reaches half of its initial value. Consequently, we propose the following criteria under which the LIP measurements on moving objects are valid:

$$\begin{aligned} &\tau_P < \tau_\gamma \\ &\tau_P < \tau_c. \end{aligned} \tag{11}$$

[1] This method can be derived with a point-wise arrangement: the distortion function, $\gamma(t,\alpha)$, is determined with Eq. (6) to be $\gamma(t,\alpha) = cos(\theta_i - \omega t)H(\theta_i+\pi/2-\omega t)/\cos(\theta_i)$, where θ_i is the position of excitation. However, this strategy reduces the signal on the PM as well as phosphorescence collection time, i.e., decreasing from $(\pi/2+\theta^+)r/\alpha u_b$ to $(\theta^+-\theta^-)r/\alpha u_b$ if the excitation point is near θ^- (see Fig. 2).

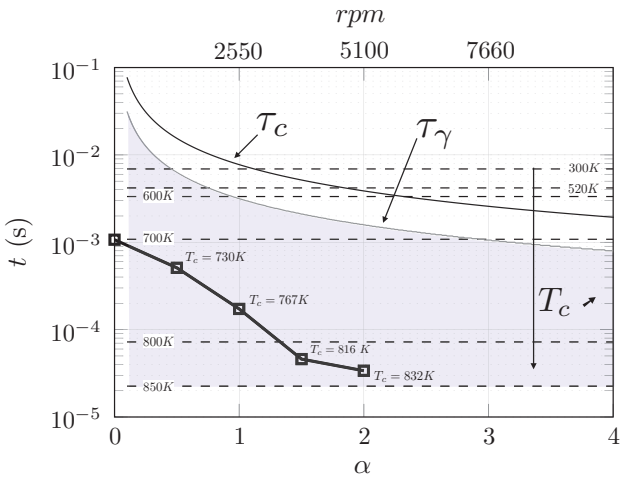

Fig. 9 Map showing the evolution of several timescales with rotation (τ_c: cylinder rotation, τ_γ: efficiency function, dotted lines: LIP). The shaded area corresponds to the range where LIP can be applied on rotating cylinders using Eq. (9)

Figure 9 represents the timescales of Eq. (11) as a function of the rotation rate α. Several phosphorescence decay times τ_P and their respective temperatures are highlighted (dashed horizontal lines). The criterion on the efficiency function τ_γ is more restrictive than the rotation timescale τ_γ. Therefore, the shaded area depicts the valid zone of measurements, where $\tau_P < \tau_\gamma$. The higher the rotation rate is, the higher the temperature of the surface needs to be to perform this type of measurements. The evolution of the cylinder temperature T_c is superimposed (black thick lines with square markers) and shows that the data of the present experiment lie within the valid range.

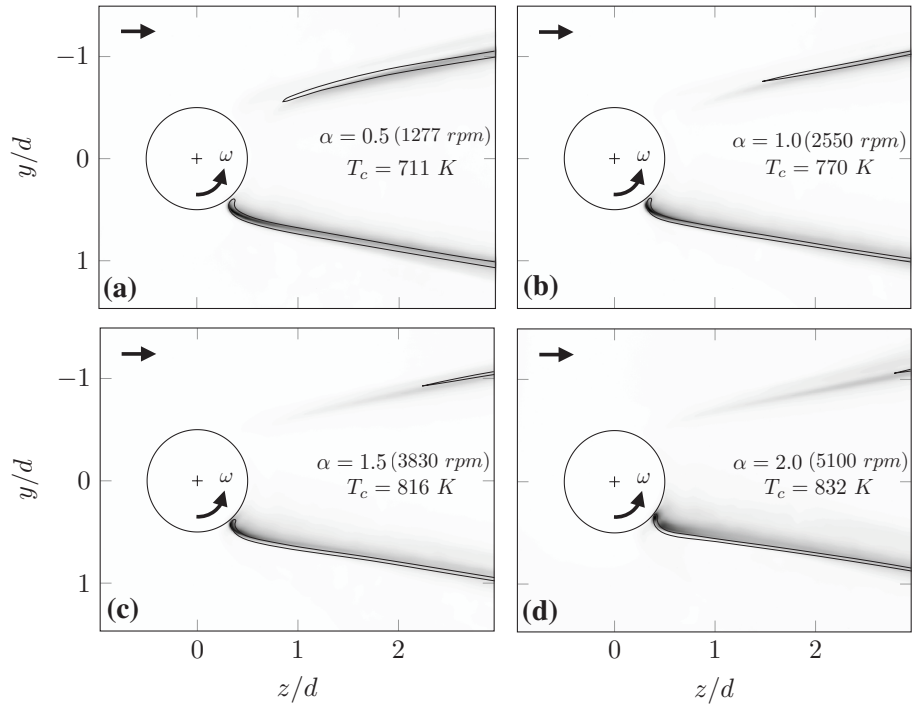

Fig. 10 Comparison between experiments (CH* chemiluminescence field) and DNS with isothermal boundary conditions (black iso-contours of 20% of the maximum heat release rate), for different rotation rates : **a** $\alpha = 0.5$, **b** $\alpha = 1.0$, **c** $\alpha = 1.5$, **d** $\alpha = 2.0$. The cylinder is fully coated with one layer

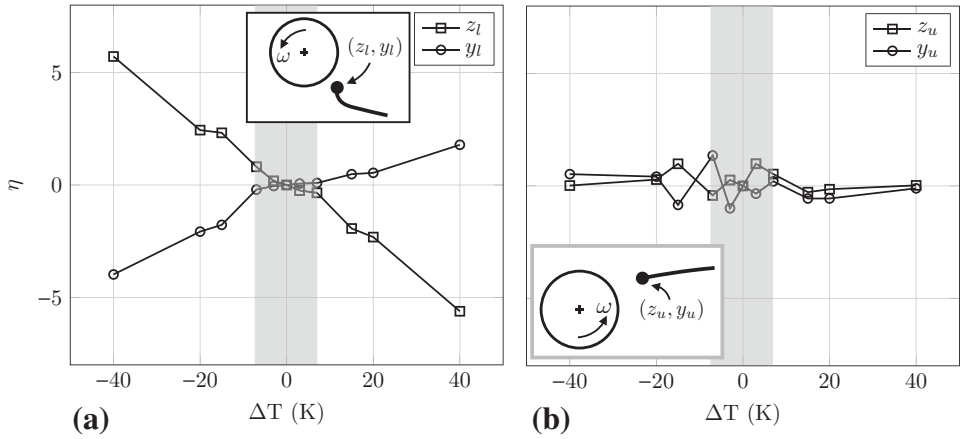

Fig. 11 Sensitivity analysis of the flame root location while varying the cylinder temperature, for the case $\alpha = 0.5$. $\Delta T = T_c^{ref} - T_c$ and $\eta = 100(x_i - x_i^{ref})/x_i^{ref}$ (x_i = z or y). Reference temperature and location are the ones obtained from Fig. 10a. **a** Lower branch. **b** Upper branch. The shaded area corresponds to the LIP precision

4.2 Validation of the temperature lumped model in numerical simulations

In contrast with previous numerical investigations, where adiabatic, coupled or lumped-adaptive conditions were implemented (Mejia et al. 2017, 2018; Xavier et al. 2017), the experimental value of the cylinder temperature is used as the boundary condition, to validate direct numerical simulations (DNS). Figure 10 shows the excellent agreement between experimental flame visualization (CH* chemiluminescence) and DNS (iso-contour of the heat release rate), for difference rotation rates α. This proves that the assumption of a uniform temperature is valid in terms of flame stabilization.

The sensitivity of the cylinder temperature on the flame root location (FRL) is evaluated by performing several DNS with a temperature shift, ΔT, ranging from −40 to 40 K (Fig. 11). The axial and radial FRL (z and y) are extracted with a crest detector on the heat release rate (set to 20% of the maximum). The spatial locations for each branch are normalized by the reference case (Fig. 10a) to give a deviation $\eta = 100(x_i - x_i^{ref})/x_i^{ref}$ ($x_i = z$ or y). The shaded area in Fig. 11 also shows the LIP precision of the present technique (i.e., ± 7K). A temperature deviation smaller than the LIP precision produces a FRL shift less than 3% for both branches. However, different trends occur when this shift is higher: the lower branch (Fig. 11a) is more sensitive to the cylinder temperature whereas the upper branch (Fig. 11b) is not affected. Indeed, as the FRL of the lower branch is

close to the cylinder, its reactivity is enhanced by the fresh gases that are pre-heated by the cylinder. In contrast, the upper branch is much more sensitive to the cylinder rotation, as depicted in Fig. 10. Therefore, in our case, a wrong estimation of the cylinder temperature could mainly lead to a change the location of the lower branch.

5 Conclusion

The accurate experimental determination of wall temperatures is crucial for the validation of numerical tools and the improvement of future combustion systems. The present work discusses the use of laser-induced phosphorescence (LIP) and shows how classical arrangements can be modified to measure the temperature of moving surfaces. Preliminary tests have been conducted to evaluate how the phosphorescent coating could affect the flame stabilization. Results show that the high temperature of the substrate does not alter the spectroscopic properties of phosphor particles, indicating that the coating can be used during several campaigns. The emissivity of the coated surface is increased by almost 40%, mainly due to the roughness increase. However, the transient and steady flame locations are weakly affected, enabling non-intrusive measurements. The classical point-wise LIP arrangement has been modified to allow temperature measurements at the surface of a moving object. A larger area is illuminated and the collected signal is corrected by a distortion function accounting for the displacement during the phosphorescence decay. The validity of this correction is assessed theoretically and experimentally. The main constraint stems from the velocity of the object and the phosphorescence decay rate. Eventually, measurements on a rotating cylindrical flame holder are compared with numerical simulations, and show an excellent agreement. A sensitivity analysis highlights that the lower branch is sensitive to the cylinder temperature, whereas the rotation rate α determines the location of the upper branch.

Acknowledgements The research leading to these results has received funding from the European Research Council under the European Union's Seventh Framework Programme (FP/2007-2013)/ERC Grant Agreement ERC-AdG 319067-INTECOCIS. The authors wish also to thank M. Marchal and S. Cazin from IMFT for their precious help with the experimental diagnostics, and Q. Douasbin (IMFT), C. Kraus (IMFT), B. Bedat (IMFT), and T. Schuller (IMFT) for useful discussions.

References

Alden M, Omrane A, Richter M, Sarner G (2011) Thermographic phosphors for thermometry: a survey of combustion applications. Prog Energy Comb Sci 37:422–461

Allison SW, Cates MR, Noel BW, Gillies GT (1988) Monitoring permanent-magnet motor heating with phosphor thermometry. IEEE Trans Instrum Meas 37:637–641

Allison SW, Gillies GT (1997) Remote thermometry with thermographic phosphors: instrumentation and applications. Rev Sci Instrum 68:2615–2650

Atakan B, Roskosch D (2013) Thermographic phosphor thermometry in transient combustion: a theoretical study of heat transfer and accuracy. Proc Combust Inst 34:3603–3610

Berger S, Richard S, Duchaine F, Staffelbach G, Gicquel LYM (2016) On the sensitivity of a helicopter combustor wall temperature to convective and radiative thermal loads. Appl Therm Eng 103:1450–1459

Brubach J, Feist JP, Dreizler A (2008) Characterization of Manganese-activated magnesium fluorogermanate with regards to thermographic phosphor thermometry. Meas Sci Technol 19(025):602–11

Brubach J, Pflitsch C, Dreizler A, Atakan B (2013) On surface temperature measurements with thermographic phosphors: a review. Prog Energy Comb Sci 39:37–60

Chambers M, Clarke D (2009) Doped Oxides for high- temperatures luminescence and lifetime thermometry. Ann Rev Mater Res 39:325–359

Dreizler A, Bohm B (2015) Advanced laser diagnostics for an improved understanding of premixed flame-wall interactions. Proc Combust Inst 35:37–64

Duchaine F, Corpron A, Pons L, Moureau V, Nicoud F, Poinsot T (2009) Development and assessment of a coupled strategy for conjugate heat transfer with large eddy simulation: application to a cooled turbine blade. Int J Heat Fluid Flow 30:1129–1141

Ezekoye OA, Greif R, Lee D (1992) Increased surface temperature effects on wall heat transfer during unsteady flame quenching. In: 24th Symp. (Int.) on Combustion. The Combustion Institute, Pittsburgh, pp 1465–1472

Facchini B, Magi A, Greco AS (2004) Conjugate heat transfer simulation of a radially cooled gas turbine vane. In: ASME Turbo Expo 2004: Power for Land, Sea, and air. American Society of Mechanical Engineers, pp 951–961

Feist JP, Heyes AL, Seefeldt S (2002) Thermographic phosphors for gas turbines: instrumentation development and measurement uncertainties. In: 11th International symposium on application of laser techniques to fluid mechanics, Lisbon, Portugal

Fuhrmann N, Brubach J, Dreizler A (2013) Phosphor thermometry: a comparison of the luminescence lifetime and the intensity ratio approach. Proc Combust Inst 34:3611–3618

Guiberti TF, Durox D, Scouflaire P, Schuller T (2015) Impact of heat loss and hydrogen enrichment on the shape of confined swirling flames. Proc Combust Inst 35:1385–1392

Hooker JA, Doorbar PJ (2000) Metal matrix composites for aeroengines. Mater Sci Technol 16:725–731

Jainski C, Ribmann M, Janicka J, Dreizler A (2017) Sidewall quenching of atmospheric laminar premixed flames studied by laser-based diagnostics. Combust Flame 183:271–282

Kashdan JT, Bruneaux G (2011) Laser-induced phosphorescence measurements of combustion chamber surface temperature on a single-cylinder diesel engine. In: SAE Technical Paper 2011-01-2049. SAE International

Khalid AH, Kontis K (2008) Thermographic phosphors for high temperature measurements: principles, current state of the art and recent applications. Sensors 8:5673–5744

Knappe C, Linden J, Nada FA, Ritcher M, Alden M (2012) Investigation and compensation of the nonlinear response in photomultiplier tubes for quantitative single-shot measurements. Rev Sci Instrum 83:034901

Kraus C, Selle L, Poinsot T, Arndt CM, Bockhorn H (2017) Influence of heat transfer and material temperature on combustion instabilities in a swirl burner. J Eng Gas Turb Power 129(051):503

Lakshmisha KN, Paul PJ, Mukunda HS (1991) On the flammability limit and heat loss in flames with detailed chemistry. In: Symposium (international) on combustion, vol 23. Elsevier, pp 433–440

Lamouroux J, Ihme M, Fiorina B, Gicquel O (2014) Tabulated chemistry approach for diluted combustion regimes with internal recirculation and heat losses. Combust Flame 161:2120–2136

Lawrence P (2009) Meeting the challenge of aviation emissions: an aircraft industry perspective. Tech Anal Strat Manag 21:79–92

Lee YK, Oh JR, Huh YRD (2007) Strong perturbation of the guided light within Y_2O_3 : Eu^{3+} thin film phosphors coated with two-dimensional air-hole photonic crystal arrays. Appl Phys Lett 91(231):908

Lefebvre AH (1999) Gas turbines combustion. Taylor & Francis, London

Lempereur C, Andral R, Prudhomme J (2008) Surface temperature measurement on engine components by means of irreversible thermal coatings. Meas Sci Technol 19(105):501

Linden J, Johansson B, Richter M, Alden M (2009) Investigation of potential laser-induced heating effects when using thermographic phosphors for gas-phase thermometry. Appl Phys B 96:237–240

Lu JH, Ezekoye O, Greif R, Sawyer F (1990) Unsteady heat transfer during side wall quenching of a laminar flame. In: 23rd Symp. (Int.) on Combustion. The Combustion Institute, Pittsburgh, pp 441–446

Mann M, Jainski C, Euler M, Bohm B, Dreizler A (2014) Transient flame-wall interactions: experimental analysis using spectroscopic temperature and CO concentrations measurements. Combust Flame 161:2371–2386

Mannick L, Brown SK, Campbell SR (1987) Phosphor-based thermometry of rotating surfaces. Appl Opt 26:4014–4017

Mejia D, Bauerheim M, Xavier P, Ferret B, Selle L, Poinsot T (2017) Stabilization of a premixed flame on a rotating cylinder. Proc Combust Inst 36:1447–1455

Mejia D, Miguel-Brebion M, Ghani A, Kaiser T, Duchaine F, Selle L, Poinsot T (2018) Influence of flame-holder temperature on the acoustic flame transfer function of a laminar flame. Combust Flame 188:5–12

Mejia D, Selle L, Bazile R, Poinsot T (2015) Wall-temperature effects on flame response to acoustic oscillations. Proc Combust Inst 35:3201–3208

Mercier R, Guiberti TF, Chatelier A, Durox D, Giquel O, Darabiha N, Schuller T, Fiorina B (2016) Experimental and numerical investigation of the influence of thermal boundary conditions on premixed swirling flame stabilization. Combust Flame 171:42–58

Miguel-Brebion M, Mejia D, Xavier P, Duchaine F, Bedat B, Selle L, Poinsot T (2016) Joint experimental and numerical study of the influence of flame holder temperature on the stabilization of a laminar methane flame on a cylinder. Combust Flame 172:153–161

Padture NP, Gell M, Jordan EH (2002) Thermal barrier coatings for gas-turbine engine applications. Science 296:280–284

Poinsot T, Veynante D (2011) Theoretical and Numerical Combustion, 3rd edn. (http://www.cerfacs.fr/elearning)

Popp P, Baum M (1997) An analysis of wall heat fluxes, reaction mechanisms and unburnt hydrocarbons during the head-on quenching of a laminar methane flame. Combust Flame 108(3):327–348

Tay-Wo-Chong L, Polifke W (2013) Large eddy simulation-based study of the influence of thermal boundary condition and combustor confinement on premix flame transfer functions. J Eng Gas Turb Power 135:021502

Tobin K, Allison S, Cates MR, Capps GL, Beashears DL, Cyr M, Noel BW (1990) High-temperature phosphor thermometry of rotating turbine blades. AIAA J 28:1485–1490

Wulff A, Hourmouziadis J (1997) Technological review of aeroengine pollutant emissions. Aerosp Sci Technol 1:557–572

Xavier P, Ghani A, Miguel-Brebion M, Bauerheim M, Selle L, Poinsot T (2017) Experimental and numerical investigation of flames stabilised behind rotating cylinders: interaction of flames with a moving wall. J Fluid Mech 813:127–151